HHS Public Access

Author manuscript

Eur J Nucl Med Mol Imaging. Author manuscript; available in PMC 2017 March 01.

Published in final edited form as:

Eur J Nucl Med Mol Imaging. 2016 March ; 43(3): 537–547. doi:10.1007/s00259-015-3209-0.

PET Imaging Evaluation of [^{18}F]DBT-10, a Novel Radioligand Specific to α_7 Nicotinic Acetylcholine Receptors, in Nonhuman Primates

Ansel T. Hillmer[1], **Ming-Qiang Zheng**[1], **Songye Li**[1], **Matthias Scheunemann**[2], **Shu-fei Lin**[1], **Daniel Holden**[1], **David Labaree**[1], **Jim Ropchan**[1], **Rodrigo Teodoro**[2], **Winnie Deuther-Conrad**[2], **Richard E. Carson**[1], **Peter Brust**[2], and **Yiyun Huang**[1]

[1]PET Center, Yale University, PO Box 208048, 801 Howard Ave, New Haven, CT 06520-8048

[2]Helmholtz-Zentrum Dresden-Rossendorf, Institute of Radiopharmaceutical Cancer Research, Permoserstraße 15, 04318 Leipzig, Germany

Abstract

Purpose—PET radioligands specific to α_7 nicotinic acetylcholine receptors (nAChRs) afford *in vivo* imaging of this receptor for neuropathologies such as Alzheimer's disease, schizophrenia, and substance abuse. This work aims to characterize the kinetic properties of an α_7-nAChR specific radioligand, 7-(1,4-diazabicyclo[3.2.2]nonan-4-yl)-2-[^{18}F]-fluorodibenzo[b,d]thiophene 5,5-dioxide ([^{18}F]DBT-10), in nonhuman primates.

Methods—[^{18}F]DBT-10 was produced via nucleophilic substitution of the *nitro*-precursor. Four *Macaca mulatta* subjects were imaged with [^{18}F]DBT-10 PET, with measurement of [^{18}F]DBT-10 parent concentrations and metabolism in arterial plasma. Baseline PET scans were acquired for all subjects. Following one scan, *ex vivo* analysis of brain tissue was performed to inspect for radiolabeled metabolites in brain. Three blocking scans with 0.69 and 1.24 mg/kg of the α_7-nAChR-specific ligand ASEM were also acquired to assess dose-dependent blockade of [^{18}F]DBT-10 binding. Kinetic analysis of PET data was performed using the metabolite-corrected input function to calculate the parent fraction corrected total distribution volume (V_T/f_P).

Results—[^{18}F]DBT-10 was produced within 90 min at high specific activities of 428±436 GBq/μmol at end of synthesis. Metabolism of [^{18}F]DBT-10 varied across subjects, stabilizing by 120 min post-injection at parent fractions of 15–55%. Uptake of [^{18}F]DBT-10 in brain occurred rapidly, reaching peak SUVs of 2.9–3.7 within 30 min. The plasma free fraction was 18.8±3.4%. No evidence for radiolabeled [^{18}F]DBT-10 metabolites was found in *ex vivo* brain tissue samples. Kinetic analysis of PET data was best described by the two-tissue compartment model. Estimated V_T/f_P values were 193–376 mL/cm^3 across regions, with regional rank order of thalamus > frontal cortex > striatum > hippocampus > occipital cortex > cerebellum > pons. Dose dependent

Corresponding Author: Dr. AT Hillmer, PO Box 208048, PET Center, 801 Howard Ave, New Haven, CT 06520-8048, ansel.hillmer@yale.edu, Phone: 203-787-2302, Fax: 203-785-3107.

Ethical Approval. All applicable international, national, and institutional guidelines for the care and use of animals were followed. All procedures performed in studies involving animals were in accordance with the ethical standards of the Yale University Institutional Animal Care and Use Committee.

blockade of [^{18}F]DBT-10 binding by structural analog ASEM was observed throughout the brain, and occupancy plots yielded a V_{ND}/f_P estimate of 20±16 mL/cm^3.

Conclusions—These results demonstrate suitable kinetic properties of [^{18}F]DBT-10 for *in vivo* quantification of α_7-nAChR binding in nonhuman primates.

Keywords

Nicotine; nicotinic acetylcholine receptor; alpha 7; PET

Introduction

Nicotinic acetylcholine receptors (nAChRs) are ligand-gated ion channels distributed throughout the central nervous system [1]. They are composed of subunits arranged in a pentameric fashion, most commonly in heteromeric $\alpha_4\beta_2$- and homomeric α_7-nAChR subtype assemblies [2]. Cerebral α_7-nAChRs have generated much interest for their role in inflammation [3], memory, and cognition [4, 5], and have been implicated in psychiatric pathologies including schizophrenia [6], Alzheimer's disease [7], depressive disorder [8], and substance abuse disorders [9, 10]. However, the role of α_7-nAChRs in these neuropathologies is not yet well understood.

Positron emission tomography (PET) radioligands specific to the α_7-nAChR provide critical tools for *in vivo* assay of receptors in disease progression and drug development. A number of α_7-nAChR radioligands have been evaluated (see [11] for review), however, only two have been advanced to PET imaging in humans (see Fig. 1). The first, [^{11}C]CHIBA-1001, exhibited high non-specific binding and poor specificity for the α_7-nAChR receptor [12, 13], with peak target-background ratios of 1.3, limiting its clinical utility. The second, [^{18}F]ASEM, exhibited preclinical binding potential (BP_{ND}) values of 3.9–6.6 with dose-dependent blockade [14], and appropriate kinetic properties for human imaging [15]. The radioligand 7-(1,4-diazabicyclo[3.2.2]nonan-4-yl)-2-[^{18}F]-fluorodibenzo[b,d]thiophene 5,5-dioxide ([^{18}F]DBT-10) is based on the same dibenzothiophene backbone as [^{18}F]ASEM. As indicated in Figure 1, our group measured higher α_7-nAChR *in vitro* binding affinities for [^{18}F]DBT-10 (K_i = 0.6 vs. 0.84 nM for [^{18}F]ASEM), with significantly greater selectivity for the α_7-nAChR relative to the more abundant $\alpha_4\beta_2$ (6,200-fold selectivity for [^{18}F]DBT-10 vs. 750-fold for [^{18}F]ASEM) and other nAChR and 5-hydroxytryptamine receptor subtypes. Thus, [^{18}F]DBT-10 may have less nonspecific binding than [^{18}F]ASEM, leading to improved imaging properties. We therefore conducted the present studies with the goal of characterizing the *in vivo* kinetic properties of [^{18}F]DBT-10 in nonhuman primates. These studies featured analysis of [^{18}F]DBT-10 in both the arterial plasma and brain tissue, including full kinetic modeling with the parent arterial input function. Blocking studies with an α_7-nAChR selective ligand were conducted to examine specific binding levels. Finally, we conducted an *ex vivo* study to inspect for radiolabeled metabolites in the brain.

Materials and Methods

Subjects

The subjects for this study were four *Maccaca mulatta* (2 females, 8–15 years old, 7–10 kg; 2 males, 6–12 years old, 10–14 kg). All experiments followed institutional guidelines and were approved by the Yale University Institutional Animal Care and Use Committee.

Radiochemistry

[^{18}F]DBT-10 was prepared from its nitro-precursor via nucleophilic displacement, as shown in Figure 2A. Target-produced [^{18}F]fluoride in [^{18}O]water was trapped by an ion-exchange cartridge and then eluted with a solution of Kryptofix-222/K_2CO_3 in MeCN/H_2O (1.4 mL). The [^{18}F]fluoride was azeotropically dried, and a solution of the nitro-precursor (1–2 mg) in DMSO (0.2 mL) was then added to the dried [^{18}F]fluoride. The solution was mixed and heated at 140 °C for 10 min. After cooling, the crude product was diluted with 1.5 mL of the semi-preparative HPLC mobile phase and loaded onto a C18 HPLC column (Phenomenex Gemini, 250 × 10 mm, 10 μm) eluting with a mixture of 40% MeCN and 60% 0.1% triethylamine at a flow rate of 5 mL/min. The product fraction, which eluted at 16–18 min, was collected and diluted in a solution of 200 mg ascorbic acid in 50 mL of deionized water (DI). The solution was then passed through a Waters Classic C18 SepPak cartridge. The SepPak was washed with a solution of 10 mg ascorbic acid in 10 mL of DI water and dried with air. The trapped product was eluted off the SepPak with 1 mL of absolute ethanol followed by a solution of 3 mg ascorbic acid in 3 mL of saline. The combined eluents were passed through a 0.22 μm Millipore membrane filter into a dose vial containing a solution of 7 mg ascorbic acid in 7 mL of saline and 0.2 mL of 4.2% $NaHCO_3$ for final formulation.

Quality control tests were performed by HPLC analysis of the product solution on a Shimadzu HPLC system equipped with both UV and radioactivity detectors to determine the chemical purity, radiochemical purity, and specific activity. HPLC conditions consisted of a YMC C18 column (250 × 4.6 mm, 5 μm), with a mobile phase of 45% acetonitrile and 55% 0.1% triethylamine at a flow rate of 2 mL/min. The identity of [^{18}F]DBT-10 product was confirmed by co-injection of the radiolabeled product solution with an authentic sample of DBT-10 and detection of co-eluted UV and radioactive peaks on the HPLC chromatogram.

PET Scanning Procedures

A total of seven PET scans were conducted. Four baseline PET scans were acquired, one for each subject; three were 240 min in duration, while 120 min of PET data were acquired for the terminal study. Three additional blocking scans were acquired in two subjects, with the α_7-nAChR specific ligand ASEM given less than 30 min prior to [^{18}F]DBT-10 injection, and PET data were subsequently acquired for 180 min.

On the day of scans, subjects were initially anesthetized with ketamine hydrochloride (10 mg/kg, intramuscular) at least 2 h prior to radiotracer administration. Subjects were then maintained on oxygen and 1.5–3% isoflurane for the duration of scans. Vital signs were continuously monitored and recorded, including respiration rate, blood pressure, heart rate, and temperature. A venous line for radiotracer administration was placed in the saphenous

vein, with an arterial line for blood sampling inserted in a radial or femoral artery on the opposite limb.

A Focus 220 PET scanner (Simens/CTI, Knoxville, TN) was used for PET data acquisition, which has an intrinsic resolution of 1.4 mm at the center of the field of view. A transmission scan was first acquired using a continuously rotating ^{137}Cs source for 9 min. [^{18}F]DBT-10 was administered as a 167–185 MBq slow bolus injection over 3 min with a Harvard syringe pump (PHD 22/2000, Harvard Apparatus, Holliston, MA). PET data were then continuously acquired in list-mode for 120–240 min. Discrete arterial blood samples were acquired throughout PET scanning, with rapid (45 s) sampling immediately post-injection and gradually slowing to 30 min sampling at the end of scans.

Arterial Input Function Measurement

Radioactivity assay of arterial blood samples was performed with a cross calibrated well-type gamma counters (Wizard 1480/2480, Perkin Elmer, Waltham, MA). Whole blood samples were assayed and centrifuged (2,930 *g* for 5 min). Supernatant plasma samples were then collected and assayed for radioactivity. Select plasma samples (drawn at 3, 8, 15, 30, 60, 90, 120, 180, 240 min post-injection) were analyzed with HPLC to measure the radioligand metabolite profile.

For metabolite analysis, plasma samples were mixed with urea to a final concentration of 8 M and filtered through 1.0 μm Whatman 13 mm CD/X filters (GE, Florham Park, NJ). Samples were then analyzed on an adapted, automatic column-switching HPLC system[16]. Upon injection, samples were first eluted through a hand-packed C18 sorbent capture column (Strata-X, Phenomenex, Torrance CA) with a mobile phase of 1% MeCN and 99% H_2O (v:v) at a flow rate of 2 mL/min for 4 min. The capture column was then back-flushed with a mobile phase of 45% acetonitrile and 55% 20 mM ammonium bicarbonate (v/v) eluted through a Phenomenex Gemini-NX analytical column (4.6 × 250 mm, 5 μm) at a flow rate of 1.65 mL/min. The eluent was collected with a fraction collector (CF-1 Fraction Collector, Spectrum Chromatography, Houston, TX) in discrete 2 min bins and counted with gamma counters.

The fraction of unmetabolized parent compound was measured as the ratio of the eluted parent compound, which had a retention time of ~11 min, to the total radioactivity collected. The time course of this parent fraction was fitted to an inverted gamma function and corrected for filtration efficiency. Finally, the input function was calculated as the product of the assayed radioactivity concentration in plasma and the unmetabolized parent fraction.

In addition, the free fraction (f_P) was determined from plasma samples with ultrafiltration techniques. An arterial blood sample (3.0 mL) drawn prior to radiotracer injection was gently mixed with ~3 kBq of [^{18}F]DBT-10. After partitioning the plasma from red blood cells via centrifugation, the plasma sample was extracted, loaded onto an ultrafiltration cartridge (Millipore Centrifree UF devices), and centrifuged at 1,228 *g* for 20 min. The free fraction was calculated as the ratio of radioactivity in the ultrafiltrate to the total radioactivity in the plasma sample. Measurements of f_P were performed in triplicate for each scan.

Ex Vivo [^{18}F]DBT-10 Study

A male *Maccaca mulatta* (12 years old, 14 kg) was injected with 183 MBq [^{18}F]DBT-10 intravenously, and PET data were acquired for 120 min. The subject was then sacrificed under isoflurane anesthesia with a lethal dose of pentobarbital after a final arterial blood sample was withdrawn. The brain was harvested and dissected, with tissue samples extracted from frontal cortex, cerebellum, hippocampus, thalamus, and putamen. Tissue samples were processed using the same procedures described previously [17] and analyzed with the following HPLC conditions: A mobile phase of 45% acetonitrile and 55% 20 mM ammonium bicarbonate (v/v) eluted through a Phenomenex Gemini-NX analytical column (5 μm, 4.6 × 250 mm) at a flow rate of 1.65 mL/min (retention time for ^{18}F-DBT-10: ~7 min).

[^{18}F]DBT-10 Blocking Studies with Cold ASEM

Three PET scans introduced blocking doses of the α_7-nAChR specific ligand ASEM[14], administered as a 15 min slow bolus with a syringe pump 17–26 min prior to [^{18}F]DBT-10 administration, to examine drug occupancy and binding specificity of [^{18}F]DBT-10 for the α_7-nAChR. Two scans were conducted with the same subject (F, 15 years old, 7 kg) to examine for dose-dependent blockade of [^{18}F]DBT-10 with ASEM doses of 0.69 and 1.24 mg/kg. A third scan was conducted in a second subject (M, 6 years old, 10 kg) with 1.24 mg/kg ASEM to compare nonspecific [^{18}F]DBT-10 binding across subjects. Data acquisition, including arterial blood sampling, then continued for 180 min as described above.

Anatomical MRI Acquisition

High-resolution T_1-weighted images were acquired for image co-registration and region of interest (ROI) identification. MR data were acquired prior to PET image acquisition with a Siemens 3T Trio scanner, with an extremity head coil in the coronal direction and the following spin echo sequence (TE = 3.34 ms, TR = 2530 ms, flip angle = 7°, thickness = 0.50 mm, field-of-view = 140 mm, image matrix = 256 × 256 × 176, voxel size = 0.547 × 0.547 × 0.500 mm). Non-brain structures were removed with FMRIB's Brain Extraction Tool (http://www.fmrib.ox.ac.uk/fsl/BET).

Image Data Processing

Raw list-mode PET data were histogrammed (frames of 6 × 0.5 min; 3 × 1 min; 2 × 2 min; and N × 5 min to scan termination) and reconstructed with Fourier rebinning followed by 2D filtered back projection, using a 0.15 mm^{-1} Shepp filter and including corrections for scanner normalization, detector deadtime, randoms, and radiation scatter and attenuation. This resulted in a reconstructed image resolution of ~3.2 mm. The PET images were then registered to MR image space with a 6-parameter rigid body registration[18]. The MR native space was normalized using nonlinear registration to a high-resolution rhesus monkey atlas[19] with BioImage Suite 3.01 (http://www.bioimagesuite.org/index.html). Time-activity curves were extracted by mapping atlas-defined regions to PET native space using the optimal transformation matrices calculated in the registration and normalization steps.

ROIs extracted included caudate, cerebellum, cingulate, frontal cortex, hippocampus, occipital cortex, pons, putamen, temporal cortex, and thalamus.

[^{18}F]DBT-10 Kinetic Analysis

For all PET scans, the primary outcome measures werethe total volume of distribution [20], both uncorrected (V_T) and corrected (V_T/f_P) by the plasma free fraction. Regional V_T values were estimated using both one-tissue (1TCM) and two-tissue (2TCM) compartment models (see [21] for review). Model suitability was compared with the corrected Akaike Information Criterion (cAIC; [22]). Additionally, the multilinear analysis method (MA1; [23]) was assessed as a more stable, data-driven analysis method. To visualize [^{18}F]DBT-10 images, MA1 was also used to calculate V_T on the voxel level.

Receptor occupancies of α_7-nAChRs by ASEM and [^{18}F]DBT-10 V_{ND}/f_P were calculated with occupancy plots using the following equation[24]:

$$\left(\frac{V_T}{f_P}\right)_{BASELINE} - \left(\frac{V_T}{f_P}\right)_{BLOCK} = Occ\left[\left(\frac{V_T}{f_P}\right)_{BASELINE} - \left(\frac{V_{ND}}{f_P}\right)\right]$$

All grey matter regions were incorporated into occupancy plots for this analysis, which assumes uniform α_7-nAChR occupancy and non-specific binding (V_{ND}/f_P) in these regions.

Results

Radiochemistry

As shown in Figure 2, radiosynthesis of [^{18}F]DBT-10 was accomplished by reaction of the nitro-precursor in DMSO with [^{18}F]KF-Kryptofix 2.2.2 at 140 °C for 10 min (Figure 2 A). Purification by semi-preparative HPLC (Figure 2B) gave [^{18}F]DBT-10 in >99% radiochemical and chemical purities (Figure 2C), with specific activities of 369±427 GBq/μmol (n=7) at end of synthesis. The average synthesis time was 80 min. For the *in vivo* PET data, specific activities at time of injection were 360±378 GBq/μmol (range 71–1080 GBq/μmol), while the terminal study administered a specific activity of 17 GBq/μmol.

[^{18}F]DBT-10 in Arterial Plasma

Analysis of radiolabeled [^{18}F]DBT-10 metabolites in arterial plasma was performed with HPLC. Radiometabolites appeared to be more polar than [^{18}F]DBT-10 (see Figure 3A). The rate of [^{18}F]DBT-10 metabolism was variable across subjects. Three subjects exhibited fast metabolism, such that ~17% parent radioligand remained in the arterial plasma at 120 min post-injection, while the other subject exhibited ~50% parent fraction (see Figure 3B). The calculated parent input functions are shown in Figure 3C. The free fraction, f_P, of [^{18}F]DBT-10 at baseline was 18.8±3.4% (n=4). Interestingly, drug blocking of α_7-nAChR increased f_P (see occupancy section).

[^{18}F]DBT-10 *ex vivo* Brain Metabolite Analysis

HPLC analysis of homogenized brain tissue samples extracted at 120 min after [^{18}F]DBT-10 injection attributed at least 98.8% of radioactivity in brain to [^{18}F]DBT-10. In contrast, [^{18}F]DBT-10 accounted for only 12.7% of the radioactivity in arterial blood (Figure 4).

[^{18}F]DBT-10 Brain Tissue Kinetics

Uptake of [^{18}F]DBT-10 in the brain occurred rapidly, peaking at SUVs of 2.9–3.7 within 30 min post-injection and followed by clearance from the brain (**see** Figure 5). Highest uptake occurred in the thalamus, and lowest in the regions of cerebellum and pons, with moderate uptake in all other regions.

Compartment modeling revealed variation among subjects of [^{18}F]DBT-10 kinetic properties, likely reflecting differences in metabolism of parent compound. The results are summarized in Table 1. Analysis of the baseline data from two subjects (M1, M3) indicated good agreement between all modeling methods (1TCM, 2TCM, and MA1 where t*=60 min), with <5% differences in V_T values across methods. In contrast, the third subject's baseline scan (M2) yielded high V_T standard errors with the 2TCM (>10%) and poor model fits with the 1TCM, thus V_T estimates from the MA1 method ($t^* = 60$ min) were used for this subject. Estimated K_1 values were consistently fast, averaging 0.64 ± 0.12 $mL \cdot cm^{-3} \cdot min^{-1}$ across regions. Regional V_T values ranged from 28.0–72.7 mL/cm^3 for the three subjects, while the free fraction corrected values (V_T/f_P) compared extremely well between subjects, ranging from 193–376 mL/cm^3. For subject M1, a V_T/f_P map was calculated on a voxel-wise basis to visualize the brain distribution of [^{18}F]DBT-10 uptake, shown in Figure 6.

Blocking Studies of [^{18}F]DBT-10

Administration of the α_7-selective ligand ASEM immediately prior to [^{18}F]DBT-10 PET scans reduced V_T values throughout the brain. Interestingly, the [^{18}F]DBT-10 free fraction in plasma (f_P) increased following cold ASEM blocking, as shown in Table 2. Using the outcome measure V_T/f_P, a dose dependent blocking relationship was observed. Notably, the rate of [^{18}F]DBT-10 metabolism was not altered by ASEM blocking. Lassen plots of grey matter regions, shown in Figure 7, yielded good linearity ($r^2 < 0.9$) for scans with high (~63%) receptor occupancy. ASEM blocked [^{18}F]DBT-10 uptake in a dose-dependent manner in the same subject (M1), as a dose of 0.69 mg/kg cold ASEM occupied 33% of receptors while 1.24 mg/kg occupied 64% of receptors. In a second subject (M2), 1.24 mg/kg of ASEM resulted in a similar receptor occupancy of 61%. Averaged across these three scans, the estimated [^{18}F]DBT-10 V_{ND}/f_P was 20±16 mL/cm^3.

Discussion

The *in vivo* measurement of α_7-nAChR binding is a critical goal for investigating neurochemical substrates of psychiatric disorders and the acetylcholine system's role in neuroinflammation. Here, we demonstrate the favorable profile of [^{18}F]DBT-10, including the absence of radiolabeled metabolites in brain; tissue uptake in brain consistent with the known distribution of α_7-nAChRs in the rhesus monkey; accurate quantification of V_T/f_P

with 180 min scans; and dose-dependent blockade of specific binding. Thus this study demonstrates suitable kinetic properties of [^{18}F]DBT-10 for quantification of α_7-nAChRs in the rhesus monkey.

The radiosynthesis of [^{18}F]DBT-10 was carried out manually. The radiotracer was produced in >99% radiochemical and chemical purity. Specific activities at time of injection were 438±436 GBq/μmol (n=6). There was a single batch of radiotracer yielding a modest specific activity of 17 GBq/μmol, however, this dose was administered in the terminal study which was precluded from kinetic analysis, as the shortened data acquisition prevented model convergence during kinetic analysis.

The analysis of arterial plasma following [^{18}F]DBT-10 administration revealed the accumulation of two radiolabeled metabolites. The major radiolabeled compound appeared more hydrophilic than parent [^{18}F]DBT-10, while the minor metabolite species was not retained on the capture column, indicating high polarity. We speculate the major metabolite to be 2-^{18}F-fluorodibenzo[b,d]thiophene 5,5-dioxide resulting from the oxidation of parent [^{18}F]DBT-10, consistent with our previous experience with the diazabicyclononane-containing α_7 nAChR radioligand NS10743 [25]. *Ex vivo* analysis of brain tissue extracted 120 min after [^{18}F]DBT-10 administration indicated the presence of exclusively parent compound. We therefore conclude that the detected radioactivity in brain tissue reflects the distribution of [^{18}F]DBT-10 and is not contaminated by radiolabeled metabolites entering the brain.

Uptake of [^{18}F]DBT-10 into brain occurred quickly and reversibly, as shown in Figure 5. The distribution of [^{18}F]DBT-10 uptake was generally consistent with known distribution of α_7-nAChRs in the rhesus monkey, as assessed by *in vitro* [^{125}I]α-bungarotoxin autoradiography [25]. One notable exception was in the basal ganglia, where higher *in vivo* uptake of [^{18}F]DBT-10 binding was observed relative to cortical structures compared to [^{125}I]α-bungarotoxin. In addition, the regional rank order of [^{18}F]DBT-10 uptake in rhesus monkeys appears consistent with that of [^{18}F]ASEM in baboons [14]. Displacement of radiotracer was observed throughout the brain following administration of α7-nAChR selective ASEM, thus a suitable reference region for simplified [^{18}F]DBT-10 modeling may not exist in the rhesus monkey. While we observed ASEM-induced decreases in [^{18}F]DBT-10 uptake in the pons, future work examining the use of alternative white matter structures for reference region modeling may be merited.

A major factor in data analysis was the dramatic differences in metabolism rates among subjects. Of the four subjects, three exhibited rapid metabolism such that 18–22% radioactivity in plasma was parent [^{18}F]DBT-10 at 1 h post-injection, while the subject with slow metabolism (M2) exhibited 65% parent [^{18}F]DBT-10 remaining at this same time point. This slow metabolism was replicated in a blocking scan, confirming the different [^{18}F]DBT-10 kinetics in the blood among the animals. Critically, these differences in subject metabolism rates still yielded comparable V_T/f_P values between subjects (<10%), demonstrating the importance of full kinetic modeling in [^{18}F]DBT-10 quantification. Slow [^{18}F]DBT-10 metabolism may have influenced modeling of the PET data, as both the 1TCM and 2TCM analysis yielded large standard errors for parameter estimates. We currently have

no validated explanation for the difference in [^{18}F]DBT-10 metabolism other than inter-subject variability. Data from more subjects may be needed to improve characterization of [^{18}F]DBT-10 metabolism across heterogeneous populations.

Blocking studies with ASEM decreased [^{18}F]DBT-10 V_T while increasing f_P (see Table 2). The use of V_T/f_P to estimate [^{18}F]DBT-10 distribution volumes yielded a dose-dependent decrease in response to ASEM blocking, in good agreement across subjects and between predicted and measured receptor occupancies. Thus correction for the free fraction of parent in plasma may be critical for accurate quantification of [^{18}F]DBT-10. The use of V_T/f_P as a more stable outcome measure than V_T has been previously reported for PET radioligands in other neurotransmitter systems [26]. Importantly, the [^{18}F]DBT-10 f_P values, ranging from 15–22% at baseline, are sufficiently large for reliable measurement, thus the need to correct for f_P should not impede the accurate quantification of [^{18}F]DBT-10 binding.

In our hands, Lassen plots exhibited reasonable linearity; however, the caudate and putamen regions of the basal ganglia consistently exhibited the greatest deviation from the linearity of other regions, thus further investigation into the uniformity of nonspecific binding may be merited. In addition, the V_{ND}/f_P values estimated with this method varied substantially. The nonspecific uptake of [^{18}F]DBT-10 was low, with V_{ND}/f_P of 20±16 mL/cm^3. This value yields BP_{ND} estimates ranging from 11.4 to 20.4 ($BP_{ND} = (V_T/V_{ND})$-1, unitless).

The chemical structure of [^{18}F]DBT-10 is similar to that of another recently reported α_7-nAChR radiotracer, [^{18}F]ASEM [14, 15]. Given the factor of 5–10 greater receptor density of $\alpha_4\beta_2$* relative to α_7-nAChRs in the rhesus monkey [27], the relative selectivity of a candidate PET radioligand for these receptors is particularly critical. *In vitro* data indicated that [^{18}F]DBT-10 had higher affinity and selectivity for the α_7 subunit than [^{18}F]ASEM, including 3.5 times higher selectivity for the α_7-nAChR over the $\alpha_4\beta_2$*-nAChR. This motivated the present study to investigate an α_7-nAChR specific radioligand with potentially less nonspecific binding. Comparing the present data to previously published reports of [^{18}F]ASEM, there appear to be similar pharmacokinetic properties between [^{18}F]DBT-10 and [^{18}F]ASEM, whereas [^{18}F]DBT-10 had specific binding values (BP_{ND}) twice of those reported for [^{18}F]ASEM in baboons and humans [14, 15]. This initial finding supports the hypothesis that [^{18}F]DBT-10 may have improved *in vivo* binding specificity for the α_7-nAChR. Given the suitability of [^{18}F]DBT-10 for quantification of α_7-nAChRs in the nonhuman primate, future studies should examine these radiotracers in the same subjects with the same data processing and analysis techniques to carefully compare their kinetic profiles.

In conclusion, [^{18}F]DBT-10 exhibits high levels of reversible specific binding with a kinetic profile suitable for accurate *in vivo* quantification of α_7-nAChR availability. Future studies are merited to examine intra-subject variations in metabolism rates and compare with other α_7-nAChR specific radioligands. [^{18}F]DBT-10 therefore may be useful for studying the role of α_7-nAChR in disease-specific paradigms.

Acknowledgments

This work was supported by NIH T32 DA022975. We thank the staff at the Yale PET Center for their expert technical assistance in support of this work. This publication was made possible by CTSA Grant Number UL1 TR000142 from the National Center for Advancing Translational Science (NCATS), a component of the National Institutes of Health (NIH). Its contents are solely the responsibility of the authors and do not necessarily represent the official view of NIH.

References

1. Hurst R, Rollema H, Bertrand D. Nicotinic acetylcholine receptors: from basic science to therapeutics. Pharmacol Ther. 2013; 137:22–54. [PubMed: 22925690]
2. Albuquerque EX, Pereira EF, Alkondon M, Rogers SW. Mammalian nicotinic acetylcholine receptors: from structure to function. Physiol Rev. 2009; 89:73–120. [PubMed: 19126755]
3. Jonge W, Ulloa L. The alpha7 nicotinic acetylcholine receptor as a pharmacological target for inflammation. Br J Pharmacol. 2007; 151:915–29. [PubMed: 17502850]
4. Leiser SC, Bowlby MR, Comery TA, Dunlop J. A cog in cognition: How the α7 nicotinic acetylcholine receptor is geared towards improving cognitive deficits. Pharmacol Ther. 2009; 122:302–11.10.1016/j.pharmthera.2009.03.009 [PubMed: 19351547]
5. Levin ED. α7-nicotinic receptors and cognition. Curr Drug Targets. 2012; 13:602–6. [PubMed: 22300026]
6. Young JW, Geyer MA. Evaluating the role of the alpha-7 nicotinic acetylcholine receptor in the pathophysiology and treatment of schizophrenia. Biochem Pharmacol. 2013; 86:1122–32.10.1016/j.bcp.2013.06.031 [PubMed: 23856289]
7. Hernandez CM, Dineley KT. alpha7 nicotinic acetylcholine receptors in Alzheimer's disease: neuroprotective, neurotrophic or both? Curr Drug Targets. 2012; 13:613–22. [PubMed: 22300028]
8. Philip NS, Carpenter LL, Tyrka AR, Price LH. The nicotinic acetylcholine receptor as a target for antidepressant drug development. The Scientific World Journal. 2012; 2012
9. Kamens H, Andersen J, Picciotto M. Modulation of ethanol consumption by genetic and pharmacological manipulation of nicotinic acetylcholine receptors in mice. Psychopharmacology. 2010; 208:613–26.10.1007/s00213-009-1759-1 [PubMed: 20072781]
10. Brunzell DH, McIntosh JM, Papke RL. Diverse strategies targeting alpha7 homomeric and alpha6beta2* heteromeric nicotinic acetylcholine receptors for smoking cessation. Ann N Y Acad Sci. 2014; 1327:27–45.10.1111/nyas.12421 [PubMed: 24730978]
11. Brust P, Peters D, Deuther-Conrad W. Development of radioligands for the imaging of α7 nicotinic acetylcholine receptors with positron emission tomography. Curr Drug Targets. 2012; 13:594–601. [PubMed: 22300025]
12. Ishikawa M, Sakata M, Toyohara J, Oda K, Ishii K, Wu J, et al. Occupancy of alpha7 Nicotinic Acetylcholine Receptors in the Brain by Tropisetron: A Positron Emission Tomography Study Using [(11)C]CHIBA-1001 in Healthy Human Subjects. Clin Psychopharmacol Neurosci. 2011; 9:111–6.10.9758/cpn.2011.9.3.111 [PubMed: 23430308]
13. Toyohara J, Sakata M, Wu J, Ishikawa M, Oda K, Ishii K, et al. Preclinical and the first clinical studies on [11C]CHIBA-1001 for mapping alpha7 nicotinic receptors by positron emission tomography. Ann Nucl Med. 2009; 23:301–9.10.1007/s12149-009-0240-x [PubMed: 19337782]
14. Horti AG, Gao Y, Kuwabara H, Wang Y, Abazyan S, Yasuda RP, et al. 18F-ASEM, a radiolabeled antagonist for imaging the alpha7-nicotinic acetylcholine receptor with PET. J Nucl Med. 2014; 55:672–7.10.2967/jnumed.113.132068 [PubMed: 24556591]
15. Wong DF, Kuwabara H, Pomper M, Holt DP, Brasic JR, George N, et al. Human brain imaging of alpha7 nAChR with [(18)F]ASEM: a new PET radiotracer for neuropsychiatry and determination of drug occupancy. Mol Imaging Biol. 2014; 16:730–8.10.1007/s11307-014-0779-3 [PubMed: 25145965]
16. Hilton J, Yokoi F, Dannals RF, Ravert HT, Szabo Z, Wong DF. Column-switching HPLC for the analysis of plasma in PET imaging studies. Nucl Med Biol. 2000; 27:627–30. [PubMed: 11056380]

17. Lin S-F, Labaree D, Chen M-K, Holden D, Gallezot J-D, Kapinos M, et al. Further evaluation of [11C]MP-10 as a radiotracer for phosphodiesterase 10A: PET imaging study in rhesus monkeys and brain tissue metabolite analysis. Synapse. 2015; 69:86–95.10.1002/syn.21792 [PubMed: 25450608]
18. Sandiego CM, Weinzimmer D, Carson RE. Optimization of PET-MR registrations for nonhuman primates using mutual information measures: a Multi-Transform Method (MTM). Neuroimage. 2013; 64:571–81.10.1016/j.neuroimage.2012.08.051 [PubMed: 22926293]
19. Rohlfing T, Kroenke CD, Sullivan EV, Dubach MF, Bowden DM, Grant KA, et al. The INIA19 Template and NeuroMaps Atlas for Primate Brain Image Parcellation and Spatial Normalization. Front Neuroinform. 2012; 6:27.10.3389/fninf.2012.00027 [PubMed: 23230398]
20. Innis RB, Cunningham VJ, Delforge J, Fujita M, Gjedde A, Gunn RN, et al. Consensus nomenclature for in vivo imaging of reversibly binding radioligands. J Cereb Blood Flow Metab. 2007; 27:1533–9.10.1038/sj.jcbfm.9600493 [PubMed: 17519979]
21. Gunn RN, Gunn SR, Cunningham VJ. Positron emission tomography compartmental models. J Cereb Blood Flow Metab. 2001; 21:635–52.10.1097/00004647-200106000-00002 [PubMed: 11488533]
22. Hurvich CM, Tsai C-L. Regression and time series model selection in small samples. Biometrika. 1989; 76:297–307.
23. Ichise M, Toyama H, Innis RB, Carson RE. Strategies to improve neuroreceptor parameter estimation by linear regression analysis. J Cereb Blood Flow Metab. 2002; 22:1271–81.10.1097/00004647-200210000-00015 [PubMed: 12368666]
24. Cunningham VJ, Rabiner EA, Slifstein M, Laruelle M, Gunn RN. Measuring drug occupancy in the absence of a reference region: the Lassen plot re-visited. J Cereb Blood Flow Metab. 2010; 30:46–50.10.1038/jcbfm.2009.190 [PubMed: 19738632]
25. Han ZY, Zoli M, Cardona A, Bourgeois JP, Changeux JP, Le Novere N. Localization of [3H]nicotine, [3H]cytisine, [3H]epibatidine, and [125I]alpha-bungarotoxin binding sites in the brain of Macaca mulatta. J Comp Neurol. 2003; 461:49–60.10.1002/cne.10659 [PubMed: 12722104]
26. Gallezot JD, Weinzimmer D, Nabulsi N, Lin SF, Fowles K, Sandiego C, et al. Evaluation of [(11)C]MRB for assessment of occupancy of norepinephrine transporters: Studies with atomoxetine in non-human primates. Neuroimage. 2011; 56:268–79.10.1016/j.neuroimage.2010.09.040 [PubMed: 20869448]
27. Kulak JM, Ivy Carroll F, Schneider JS. [125I]Iodomethyllycaconitine binds to α7 nicotinic acetylcholine receptors in monkey brain. Eur J Neurosci. 2006; 23:2604–10.10.1111/j.1460-9568.2006.04804.x [PubMed: 16817863]
28. Ding M, Ghanekar S, Elmore CS, Zysk JR, Werkheiser JL, Lee CM, et al. [(3)H]Chiba-1001(methyl-SSR180711) has low in vitro binding affinity and poor in vivo selectivity to nicotinic alpha-7 receptor in rodent brain. Synapse (New York, NY). 2012; 66:315–22.10.1002/syn.21513
29. Hashimoto K, Nishiyama S, Ohba H, Matsuo M, Kobashi T, Takahagi M, et al. [11C]CHIBA-1001 as a novel PET ligand for alpha7 nicotinic receptors in the brain: a PET study in conscious monkeys. PloS one. 2008; 3:e3231.10.1371/journal.pone.0003231 [PubMed: 18800169]

	Affinity (K_i in nM)				% Inhibition
Compound	α_7[a]	$\alpha_4\beta_2$[b]	$\alpha_3\beta_4$[b]	$\alpha_6\beta_2$[c]	5-HT_3[d]
[^{11}C]CHIBA-1001	160 ± 15[e]	N.A.	N.A.	N.A.	14%[f]
[^{18}F]ASEM	0.84 ± 0.16	211 ± 108	42.3 ± 4.73	435 ± 152	42%
[^{18}F]DBT-10	0.60 ± 0.44	517 ± 375	119 ± 29.0	589 ± 217	2%

Figure 1.

Chemical structures and *in vitro* binding profiles of α_7-specific PET radioligands. [a]Human α_7 nAChR in stably transfected SH-SY5Y cells, with [^{3}H]methyllycaconitine as radioligand. [b]Human $\alpha_4\beta_2$ and $\alpha_3\beta_4$ nAChR in stably transfected HEK-293 cells, with [^{3}H]epibatidine as radioligand. [c]Rat $\alpha_6\beta_2$* nAChR obtained from rat striatum by immunoimmobilization using anti-rα_6 nAChR antibody, with [^{3}H]epibatidine as radioligand. [d]Percentage of inhibition at 0.1 μM concentration of test compound. [e]Taken from [28]. [f]Taken from [29].

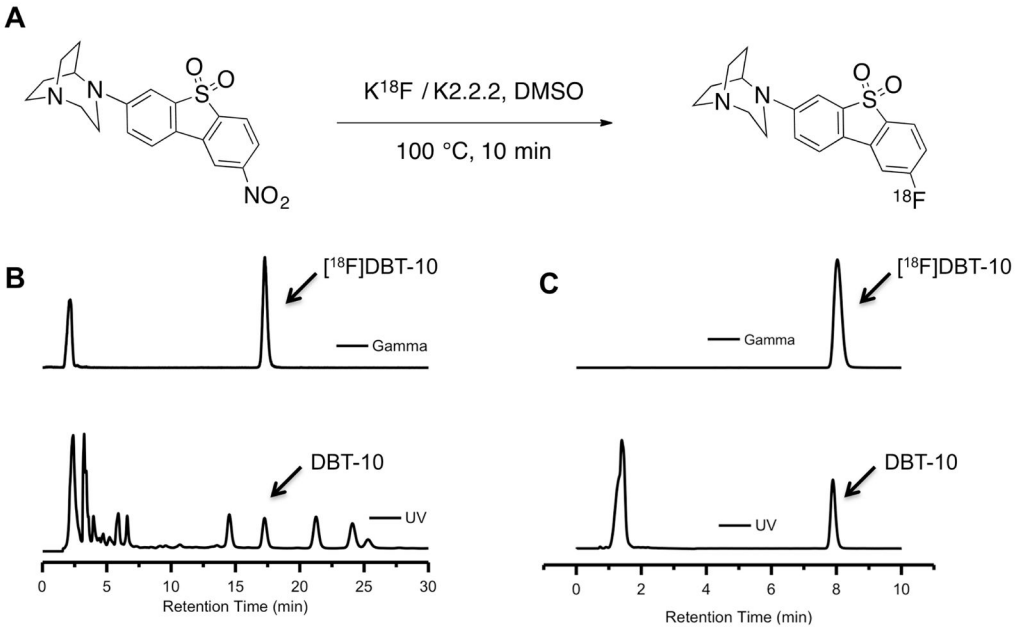

Figure 2.

Radiosynthesis of the α_7-specific compound [^{18}F]DBT-10. **A**. Radiolabeling conditions. **B**. Semi-preparative HPLC traces showing purification of [^{18}F]DBT-10, which elutes at ~17 min. **C**. Analytical HPLC traces from an injection of [^{18}F]DBT-10 product solution. The UV peak at ~1.4 min is from the presence of ascorbic acid in the product solution.

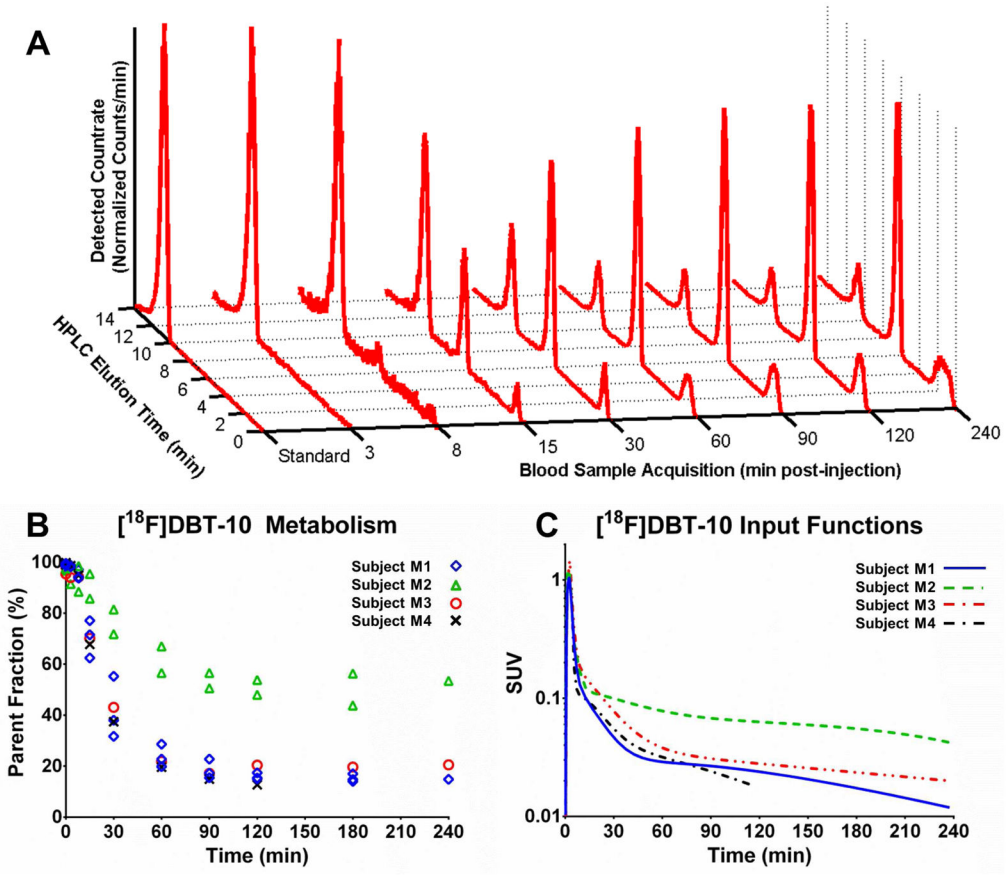

Figure 3.

[^{18}F]DBT-10 in the arterial plasma. **A.** Radio-HPLC traces for subject M1's baseline scan, with [^{18}F]DBT-10 at ~11 min and metabolites at ~1 min and ~7 min. **B.** Measured [^{18}F]DBT-10 parent fractions for all acquired scans. The three subjects are identified by separate symbols; M1: ⋄, M2: △,M3:○, M4:×. **C.** [^{18}F]DBT-10 input functions for all baseline scans, in units of SUV (activity normalized by injected dose and subject weight). The three subjects are identified by separate lines: M1, solid; M2, dashed; M3, dash-dot, red; M4, dash-dot, black.

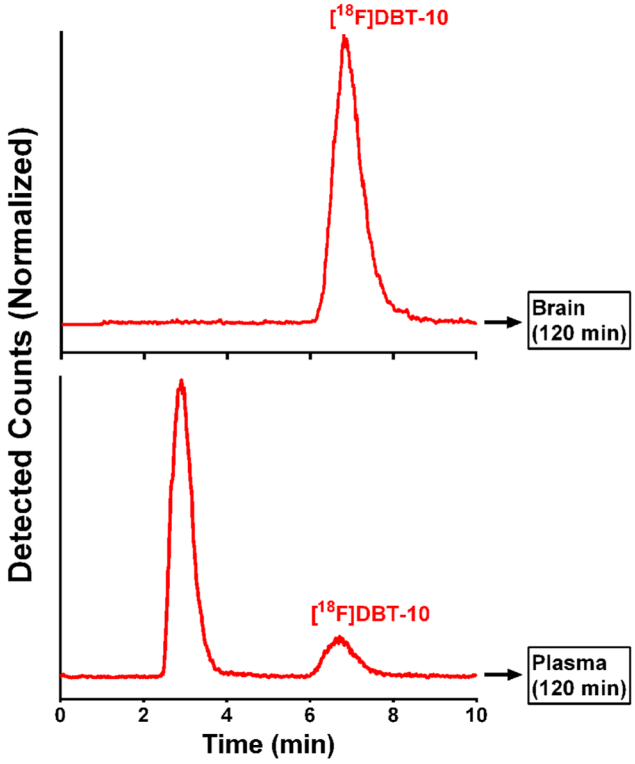

Figure 4.

Ex vivo metabolite analysis of [^{18}F]DBT-10 in brain and blood showing typical HPLC traces of radioactivity from extracted brain tissue (hippocampus) (top), and from an arterial plasma sample drawn immediately prior to animal sacrifice (bottom). For the plasma sample, t=0 represents the beginning of back-flush from the capture column.

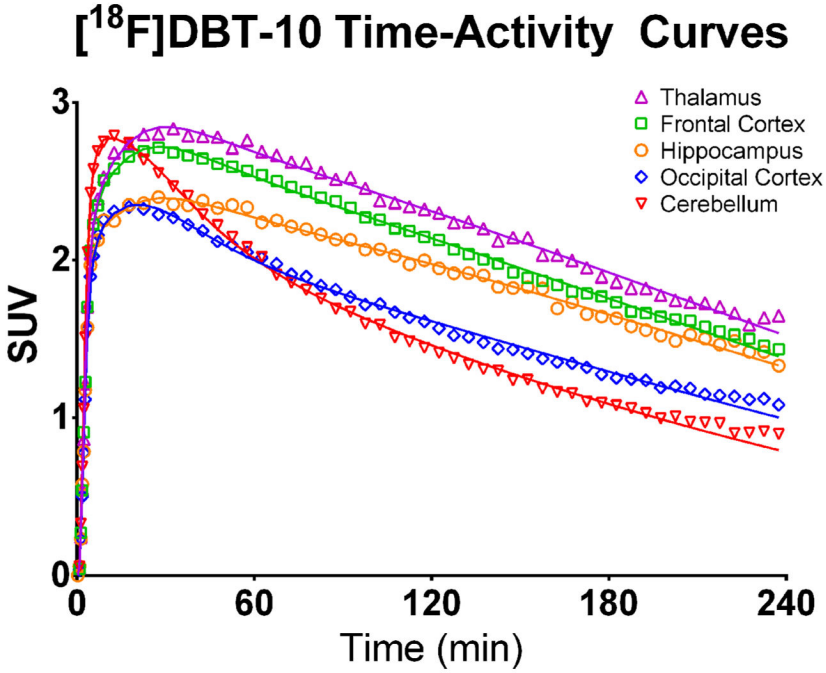

Figure 5.

[^{18}F]DBT-10 time activity curves. Values are expressed in SUV (radioactivity concentration/i.d. × weight × 1,000). Open symbols are the measured concentrations, while solid lines show the preferred 2TCM fit. Regions shown include thalamus (▲), frontal cortex (□), hippocampus (○), occipital cortex (⋄), and cerebellum (▼).

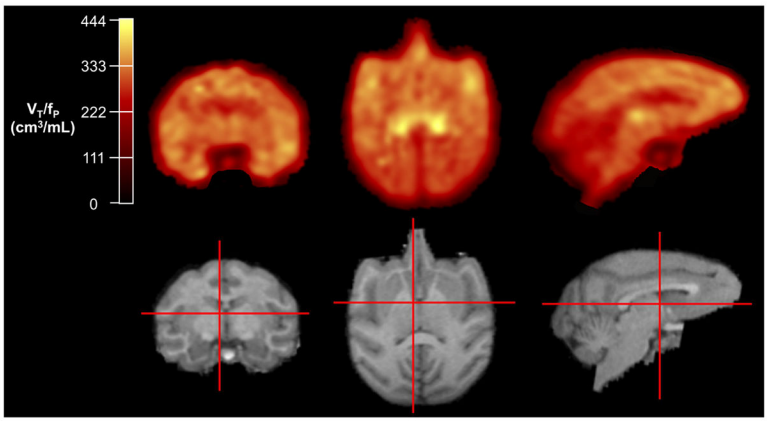

Figure 6.

[^{18}F]DBT-10 uptake in the brain of a rhesus monkey. Top: images of [^{18}F]DBT-10 V_T/f_P calculated on a voxel-wise basis using MA1 (t* = 60 min); Bottom: corresponding MRI images with red crosshairs for orientation.

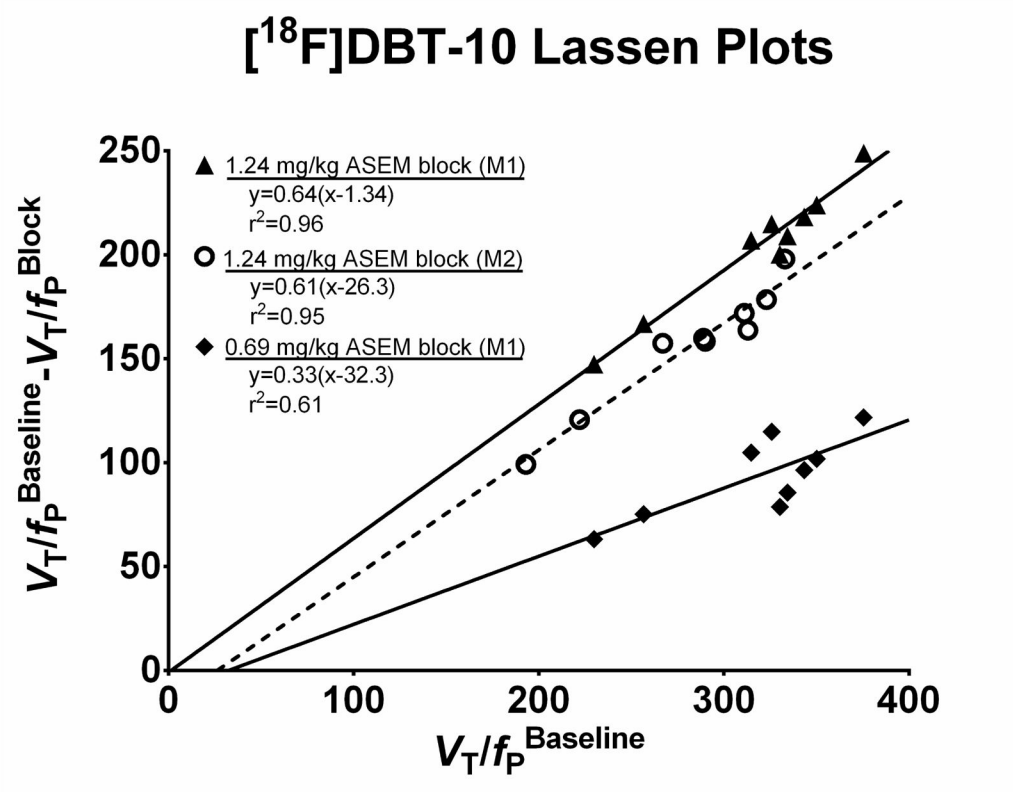

Figure 7.

[^{18}F]DBT-10 Lassen plots with cold ASEM blocking. Optimal linear fit r^2 and parameters are shown, where the slope represents fractional occupancy and x-intercept corresponds to V_{ND}/f_P. ASEM dose-dependently blocked [^{18}F]DBT-10 binding. The blocking drug ASEM was administered in doses of 0.69 mg/kg (◆) and 1.24 mg/kg (▲) for M1 and 1.24 mg/kg (○) for M2.

Eur J Nucl Med Mol Imaging. Author manuscript; available in PMC 2017 March 01.

Table 1

[^{18}F]DBT-10 Kinetic Modeling

Baseline total distribution volumes (V_T, mL/cm^3) in brain regions, with and without correction for the free fraction, are shown using two-tissue compartment model (2TCM, left), one-tissue compartment model (1TCM, center), and multilinear analysis (MA1, right) methods. Estimated K_1 values (mL·cm^{-3}·min^{-1}) from 2TCM analysis, and biases of 1TCM and MA1 to the preferred 2TCM, are also included.

		2TCM			1TCM			MA1		
		V_T	V_T/f_P	K_1	V_T	V_T/f_P	% Bias	V_T	V_T/f_P	% Bias
M1	Caudate	60.3	335	0.74	59.2	328	−1.9%	60.3	334	−0.1%
	Cerebellum	41.0	228	0.83	39.3	218	−4.3%	41.4	230	0.9%
	Cingulate	63.1	350	0.71	61.4	341	−2.7%	63.1	350	0.0%
	Frontal Cortex	61.9	344	0.68	60.7	337	−2.0%	61.9	343	−0.1%
	Hippocampus	58.6	325	0.65	57.0	316	−2.7%	58.7	326	0.2%
	Occipital Cortex	46.3	257	0.62	44.3	246	−4.5%	46.3	257	−0.2%
	Pons	46.1	256	0.46	42.9	238	−6.9%	44.1	245	−4.3%
	Putamen	59.5	330	0.74	58.4	324	−1.8%	59.5	330	0.1%
	Temporal Cortex	56.6	314	0.59	55.3	307	−2.3%	56.7	315	0.2%
	Thalamus	67.8	376	0.68	66.8	370	−1.5%	67.7	376	−0.1%
M2	Caudate	50.0*	346*	0.68	37.5*	259*	N/A	41.9	290	N/A
	Cerebellum	36.5*	252*	0.78	24.9*	172*	N/A	28.0	193	N/A
	Cingulate	56.3*	389*	0.65	41.3*	285*	N/A	45.3	313	N/A
	Frontal Cortex	58.9*	407*	0.74	42.6*	294*	N/A	46.8	323	N/A
	Hippocampus	43.5*	301*	0.53	34.9*	241*	N/A	38.6	267	N/A
	Occipital Cortex	43.5*	301*	0.72	28.3*	196*	N/A	32.1	222	N/A
	Pons	33.0*	228*	0.48	26.8*	185*	N/A	28.7	198	N/A
	Putamen	53.8*	372*	0.85	40.0*	277*	N/A	45.0	311	N/A
	Temporal Cortex	49.7*	343*	0.62	38.3*	265*	N/A	41.8	289	N/A
	Thalamus	57.6*	398*	0.81	44.5*	308*	N/A	48.2	333	N/A
M3	Caudate	60.4	271	0.64	59.1	265	−2.2%	60.2	270	−0.3%

		2TCM			1TCM			MA1		
		V_T	V_T/f_P	K_1	V_T	V_T/f_P	% Bias	V_T	V_T/f_P	% Bias
	Cerebellum	47.0	211	0.79	45.2	203	−3.8%	47.0	211	0.1%
	Cingulate	68.7	309	0.49	68.7	309	0.0%	67.3	302	−2.1%
	Frontal Cortex	71.0	319	0.51	71.0	319	0.0%	69.2	311	−2.6%
	Hippocampus	64.8	291	0.52	63.4	285	−2.1%	64.0	287	−1.2%
	Occipital Cortex	53.7	241	0.63	51.5	231	−4.1%	53.3	239	−0.7%
	Pons	50.5	227	0.37	48.1	216	−4.7%	49.6	223	−1.7%
	Putamen	59.0	265	0.62	58.4	262	−0.9%	59.0	265	−0.1%
	Temporal Cortex	64.3	289	0.45	64.3	289	0.0%	63.3	284	−1.5%
	Thalamus	72.7	326	0.52	72.7	326	0.0%	72.1	324	−0.9%

* Indicates poor model fit, where the standard error of parameter estimates was >10%.

Eur J Nucl Med Mol Imaging. Author manuscript; available in PMC 2017 March 01.

Table 2

[^{18}F]DBT-10 Blocking

Results from blocking [^{18}F]DBT-10 uptake with cold ASEM. V_T/f_P values were estimated with MA1, t*=60 min. Estimated V_{ND}/f_P and receptor occupancies, calculated with the Lassen Plots shown in Figure 7, are also presented.

Subject		**M1**			**M2**	
ASEM Dose		**Baseline**	**0.69 mg/kg**	**1.24 mg/kg**	**Baseline**	**1.24 mg/kg**
f_P		**18.0%**	**20.1%**	**41.2%**	**14.5%**	**31.7%**
V_T/f_P (mL/cm^3)	Caudate	334	249	125	290	132
	Cerebellum	230	167	83	313	149
	Cingulate	350	248	126	267	110
	Frontal Cortex	343	247	125	323	145
	Hippocampus	326	211	111	222	101
	Occipital Cortex	257	181	90	311	139
	Putamen	330	252	130	193	94
	Temporal Cortex	315	210	108	289	129
	Thalamus	376	254	127	333	135
Lassen Plots	Occupancy	-	33%	64%	-	61%
	V_{ND}/f_P (mL/cm^3)	-	32	1	-	26